

## Phase diagram of $S=1$ XXZ chain with next-nearest neighbor interaction

TAKAHIRO MURASHIMA<sup>1</sup>, KEIGO HIJII<sup>1</sup>, KIYOHIDE NOMURA<sup>1</sup> and TAKASHI TONEGAWA<sup>2</sup>

<sup>1</sup>*Department of Physics, Kyushu University, Fukuoka 812-8581, Japan*

<sup>2</sup>*Department of Mechanical Engineering, Fukui University of Technology, Fukui 910-8505, Japan*

The one dimensional  $S = 1$  XXZ model with the next-nearest-neighbor interaction  $\alpha$  and the anisotropy  $\Delta$  is studied by the numerical diagonalization. We study the ground state phase diagram of this model by the level spectroscopy method with the twisted boundary method, the phenomenological renormalization group method, the spin wave theory, the non-linear  $\sigma$  model and the renormalization group. We determine the phase boundaries among the XY phase, the Haldane phase, the ferromagnetic phase and the Néel phase and we confirm the universality class.

KEYWORDS: spin-1, ground state phase diagram, frustration, diagonalization, levelspectroscopy, non-linear  $\sigma$  model

### 1. Introduction

One dimensional antiferromagnetic Heisenberg spin chains have been the subject of recent investigations. There are no ordered ground states with the continuous symmetry breaking in the one dimensional quantum spin systems, because of the quantum fluctuation and the low dimensionality. From the Haldane conjecture,<sup>1,2</sup> it is well known that there is a fundamental difference between half-integer and integer spin chains in their low-lying excitations. In some lattice systems, the frustration, which is geometrically represented by the triangular lattice, tends to the systems disordered. We expect that the competing systems between the quantum fluctuation and the frustration plus the low dimensionality exhibit fascinating phenomena in their ground states and low-lying excitations. Recently, the  $S = 1$  spin chain materials with the next-nearest-neighbor interaction has been reported experimentally ( $\text{CaV}_2\text{O}_4$ ,<sup>3</sup>  $\text{NaV}(\text{WO}_4)_2$ <sup>4</sup>).

In this paper, we study the  $S = 1$  XXZ chain with the next-nearest-neighbor interaction, which is described by the following Hamiltonian:

$$\begin{aligned} \mathcal{H} = & \sum_{i=1}^L (S_i^x S_{i+1}^x + S_i^y S_{i+1}^y + \Delta S_i^z S_{i+1}^z) \\ & + \alpha \sum_{i=1}^L (S_i^x S_{i+2}^x + S_i^y S_{i+2}^y + \Delta S_i^z S_{i+2}^z), \end{aligned} \quad (1)$$

where  $\alpha$  is the next-nearest-neighbor interaction and  $L$  is the system size ( $L$  even). The periodic boundary condition (PBC) is assumed unless specifically mentioned.

The phase diagram of this model has been studied by the exact diagonalization for  $|\Delta| < 2$  and  $0 \leq \alpha < 0.3$  region<sup>5</sup> and the infinite-system density matrix renormalization group method (DMRG) for  $\Delta \geq 0$  and  $\alpha \geq 0$  region.<sup>6,7</sup> Many phases of the ground state have been found there; the Haldane phase, the double Haldane phase, the Néel phase, the double Néel phase, the gapped chiral phase and the gapless chiral phase. The Haldane state has an energy gap, where the spin correlation decreases exponentially as  $L \rightarrow \infty$ . The Néel state is characterized by the twofold degenerate ground state, where the staggered magnetization exhibits a long range order. In the double Haldane phase, the system can be regarded as two Haldane subchains because of the competition between the strong next-nearest-neighbor interaction and the weak nearest-neighbor interaction.<sup>8,9</sup> There exists a first order phase transition between the Haldane and the double Haldane phase.<sup>8,9</sup> We can also regard the double Néel state as two Néel subchains (up-down-up-down or up-up-down-down). The gapped chiral and the gapless chiral state has a chiral long range order, whereas the two spin correlation decays exponentially and algebraically.<sup>6,7</sup>

On the  $\alpha = 0$  line, it is known that four different ground states exist; the ferromagnetic ( $\Delta \leq -1$ ), the XY ( $-1 \leq \Delta \leq 0$ ), the Haldane ( $0 \leq \Delta \lesssim 1.17$ ) and the Néel ( $1.17 \gtrsim \Delta$ ).<sup>10-13</sup> The ferromagnetic state has a long range order of the magnetization. In the XY phase, the spin correlation shows an algebraic decay, and the correlation length is infinite. There occurs a first order phase transition between the ferromagnetic and the XY phase, and the 2D-Ising type phase transition occurs between the Haldane and the Néel phase.<sup>13</sup>

At the  $\Delta = 0$  and  $\alpha = 0$  point,<sup>10</sup> there occurs the Berezinskii-Kosterlitz-Thouless (BKT) transition which is the infinite-order transition in the traditional classification. On this transition point, the logarithmic correction appears in the the correlation function and the critical dimension and so on. This particular point is determined as the BKT transition point from the bosonization study for spin- $s$  XY model with the next-nearest-neighbor interaction<sup>14</sup> in the  $S = 1$  case. Moreover, from the other model study (with uniaxial single-ion-type anisotropy,<sup>12</sup> and with bond alternation<sup>10,11</sup>), the BKT transition occurs at  $\Delta = 0$  (of course,  $\alpha = 0$ ). Recently, it has been proved analytically that this point ( $\Delta = \alpha = 0$ ) is the BKT transition point.<sup>15</sup>

For many years, it was a difficult problem to determine numerically the critical point and the universality class of the BKT transition, because of logarithmic corrections and the slow divergence of the correlation length. This problem was successfully resolved by the level spectroscopy,<sup>16,17</sup> based on the conformal field theory and the renormalization group. Moreover, this method was improved by the twisted boundary method.<sup>18,19</sup> We use the level spectroscopy<sup>16,17</sup> with the twisted boundary method<sup>18,19</sup> to determine the BKT transition point for  $\Delta \neq 0$  or  $\alpha \neq 0$  region.

In this work, we present the phase diagram of the  $S = 1$  XXZ model analyzing the

diagonalization data by the level spectroscopy method,<sup>16,17</sup> the twisted boundary method,<sup>18,19</sup> the phenomenological renormalization group (PRG) method,<sup>20,21</sup> the spin wave theory and the renormalization group.

This paper is organized as follows. In the next section, the obtained phase diagram is presented. The numerical methods to determine the phase boundaries are explained in Sec. 3. In Sec. 4, we map eq. (1) onto the non-linear  $\sigma$  model, and we examine the phase diagram analytically. It is difficult to determine the phase diagram numerically near  $\Delta = 1$  for  $\alpha \ll 0$ . The final section is devoted to a summary and discussion.

## 2. Phase diagram

The obtained phase diagram is summarized in Fig. 1. The ground state phase diagram of this model consists of the ferromagnetic phase, the XY phase, the Haldane phase, the double Haldane phase, the gapped chiral phase, the gapless chiral phase, the Néel phase and the double Néel phase. These phases are almost determined by the infinite-system DMRG method.<sup>6,7</sup> There remains, however, the problem of the BKT transition between the XY phase and the Haldane phase. Because of the singular behavior of the BKT transition, it is difficult to determine the transition line by the DMRG method.

We determine the BKT transition line by using the level-spectroscopy method and the twisted boundary method. Then, from the finite size diagonalization data analysis, we determine the first order phase transition line between the ferromagnetic and the XY phase, and also between the ferromagnetic and the Haldane phase. Moreover, the Haldane-Néel transition line is determined by the PRG method.

Above the  $\alpha > 0.4$  region in Fig. 1, there can be the gapped and gapless chiral phase, the double Haldane phase and the double Néel phase. Since these phases have not been determined from our numerical analysis yet, we omit them from Fig. 1. However, these phases should exist because they are supported numerically and analytically.<sup>6-9</sup> This point will be discussed further in Sec.5.

## 3. Numerical Methods and Results

### 3.1 Level spectroscopy and BKT transition

In this section, we briefly review the level spectroscopy<sup>16,19</sup> and the twisted boundary method.<sup>18,19</sup>

From the bosonization method,<sup>22</sup> the one dimensional XXZ spin systems can be mapped onto the following sine-Gordon model (in Euclidean space-time)

$$S = \frac{1}{2\pi K} \int d\tau dx \{ (\partial_\tau \phi)^2 + (\partial_x \phi)^2 \} + \frac{y_2}{2\pi a^2} \int d\tau dx \cos \sqrt{2}\phi, \quad (2)$$

where  $a$  is the lattice constant. After the scaling transformation  $a \rightarrow e^{dl}a$ , we have the following

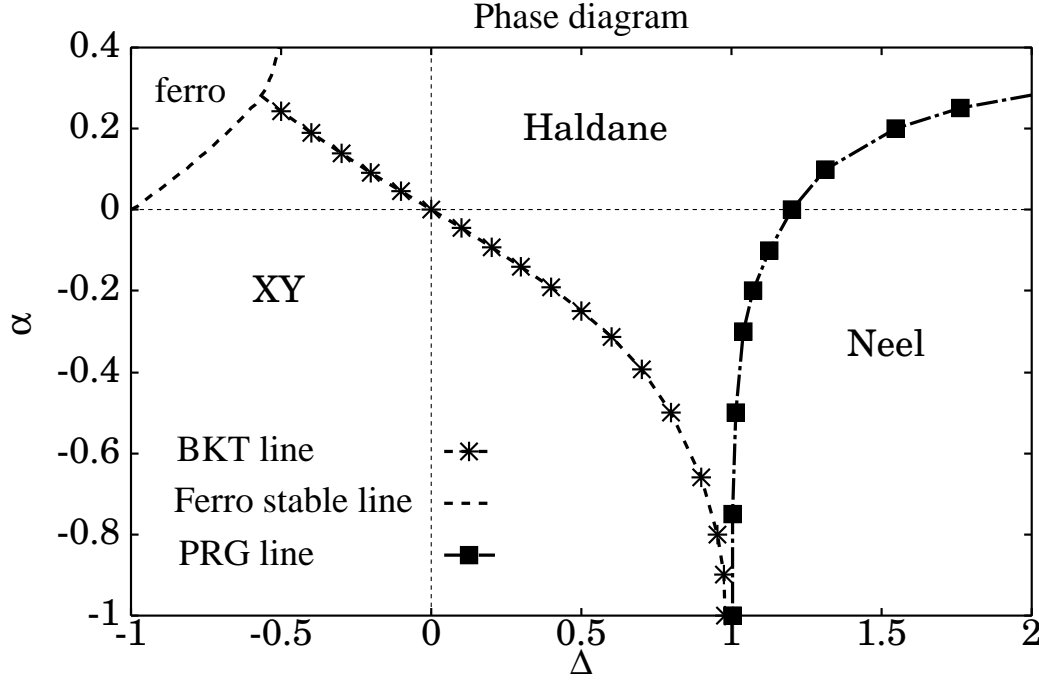


Fig. 1. The phase diagram of the  $S=1$  XXZ chain with next-nearest-neighbor interaction for  $|\Delta|$  and  $|\alpha|$  are small region. Above the  $\alpha > 0.4$  region, we are not examining because of the difficulty of the incommensurability. Though, we will investigate the ferromagnetic stable line in this region later. In the  $\alpha > 0.4$  and  $\Delta > -0.5$  region, however, there should exist the double Haldane, the double Néel, the gapped chiral and the gapless chiral phase, supported by the DMRG method.<sup>6-9</sup>

renormalization group equations:

$$\frac{dK^{-1}}{dl} = \frac{1}{8}y_2^2, \quad \frac{dy_2}{dl} = \left(2 - \frac{K}{2}\right)y_2. \quad (3)$$

$y_2$  term in eq. (2) is an irrelevant field for  $K > 4$  and relevant for  $K < 4$ . On the  $K = 4$  line, the BKT transition occurs. Denoting  $K = 4 + 2y_1$  near  $K = 4$ , we have

$$\frac{dy_1(l)}{dl} = -y_2(l)^2, \quad (4)$$

$$\frac{dy_2(l)}{dl} = -y_1(l)y_2(l), \quad (5)$$

and the renormalization flow separatrix is  $y_1^2 - y_2^2 = 0$  ( $y_1 > 0$ ). These differential equations are the famous Kosterlitz equations.<sup>23</sup> When  $y_1 > 0$ ,  $y_2$  term is irrelevant. On the other hand, when  $y_1 < 0$ ,  $y_2$  term is relevant and the scaling dimension  $x$  should be corrected as  $x \rightarrow x + Cy_2$ . Since the behavior of some scaling dimensions is different between  $y_2$  relevant field and  $y_2$  irrelevant field, thus we expect that the BKT transition point can be determined by examining the scaling dimension.

In the massless regions, the  $\cos\sqrt{2}\phi$  operators ( $y_2$  term) in the Hamiltonian (2) are irrel-

evant. Now, we introduce the vertex operator,

$$V_{n,m} = \exp(in\sqrt{2}\theta) \exp(im\sqrt{2}\phi), \quad (6)$$

where the dual field  $\theta(\tau, x)$  to  $\phi$  is defined as

$$\partial_\tau \phi(\tau, x) = -\partial_x(iK\theta), \quad \partial_x \phi(\tau, x) = \partial_\tau(iK\theta). \quad (7)$$

Then, for the free field case ( $y_2 = 0$ ), the scaling dimensions are<sup>24</sup>

$$x_{n,m} = \frac{1}{2} \left( \frac{n^2}{K} + Km^2 \right). \quad (8)$$

From the conformal field theory, the eigenvalues  $E_{n,m}$  with PBC are related to the scaling dimensions  $x_{n,m}$  as<sup>25</sup>

$$E_{n,m}(L) - E_g(L) = \frac{2\pi v_s x_{n,m}}{L} \quad (9)$$

in the limit of  $L \rightarrow \infty$ , where  $E_g(L)$  is the ground state energy for size  $L$  system under PBC, and  $v_s$  is the spin wave velocity.

From eqs. (8) and (9),

$$x_{\pm 4,0} = x_{0,\pm 1} \quad (10)$$

when  $K = 4$  and  $y_2 = 0$  (marginal). Thus we can use these energy level crossing to determine the BKT transition point.<sup>16</sup>

Though it is enough to determine the BKT transition point, there is the better method, the twisted boundary method.<sup>11</sup> This method is based on the  $SU(2)/Z_2$  symmetry on the BKT transition point. We use the following twisted boundary condition:

$$S_{L+j}^{x,y} = -S_j^{x,y}, S_{L+j}^z = S_j^z, \quad (11)$$

which can improve the original level spectroscopy method. The scaling dimensions of the eigenvalues  $E_{n,m}^{TBC}(L)$  with twisted boundary condition are

$$x_{n,m}^{TBC} = \frac{1}{2} \left\{ \frac{n^2}{K} + K \left( m + \frac{1}{2} \right)^2 \right\}, \quad (12)$$

or

$$E_{n,m}^{TBC}(L) - E_g(L) = \frac{2\pi v_s}{L} x_{n,m}^{TBC}. \quad (13)$$

Thus we can interpret this as the half-integer magnetic charge effectively. At the BKT critical point, from eqs. (8) and (12),

$$x_{2,0} = x_{0,0}^{TBC} \quad (14)$$

since  $K = 4$ . We can identify the correspondence between the operators in the boson representation and the eigenstates of spin chains by comparing their symmetry properties<sup>11,17</sup> as shown in TABLE I. The Hamiltonian (1) with the PBC is invariant under spin rotation around the z-axis, translation ( $\mathbf{S}_i \rightarrow \mathbf{S}_{i+1}$ ) and space inversion ( $\mathbf{S}_i \rightarrow \mathbf{S}_{N-i+1}$ ). Corresponding

Table I. This table shows relations between quantum numbers  $(M, P, k)$  and renormalized scaling dimensions  $x$ .  $M = \sum_{i=1}^L S_i^z$ . BC represents boundary conditions. PBC means the periodic boundary condition and TBC means the twisted boundary condition. Under the twisted boundary condition, the parity is different from that of periodic boundary condition, so we use \* to classify.  $y$  means the logarithmic correction :  $y = 1/\ln L$ .

$M$	BC	$P$	$k$	correction in $x$	operator in s.G.	scaling dimension
$\pm 2$	PBC	1	0	$1/2 - y_1(l)/4$	$\exp(\pm i 2\sqrt{2}\theta)$	$x_{\pm 2,0}$
0	TBC	-1*		$1/2 + y_1(l)/4 - y_2(l)/2$	$\sin(\phi/\sqrt{2})$	$x_{0,0,odd}^{TBC}$
0	TBC	1*		$1/2 + y_1(l)/4 + y_2(l)/2$	$\cos(\phi/\sqrt{2})$	$x_{0,0,even}^{TBC}$

eigenvalues are  $M \equiv \sum_{i=1}^N S_i^z$ ,  $k = 2\pi n/N$  ( $n = 0, \dots, N/2 - 1$ ) and  $P = \pm 1$  respectively. They are good quantum numbers to distinguish the excitation energy levels.

From TABLE I,  $x_{2,0}$  corresponds to the lowest excitation energy with  $M = \pm 2$ ,  $P = 0$ ,  $k = 0$  in terms of the spin chains, and  $x_{0,0,odd}^{TBC}$ , to the lowest excitation energy with  $M = 0$ ,  $P = -1^*$  and the twisted boundary condition. The energy level crossing between these two energies is shown in Fig. 2. Considering the  $x = 4$  irrelevant field operator  $L_{-2}\bar{L}_{-2}$  in terms of the conformal field theory,<sup>26</sup> we extrapolate the critical point as

$$\alpha(L) = \alpha_c + C_1/L^2 + C_2/L^4. \quad (15)$$

The BKT transition point is determined as shown in Fig. 3. The same procedure can be carried out varying  $\alpha$  with fixed  $\Delta$ .

Next, to check the consistency of the BKT transition, we check two universal relations, the central charge  $c$  and the energy gap ratio, as shown in Figs. 4 and 5.

The BKT transition line is expected to be described by the conformal field theory with the central charge  $c = 1$ . Here we will estimate the value of  $c$ . It is well known that the finite size correction to the ground state energy is related to the central charge  $c$  and the spin wave velocity  $v_s$  as follows,<sup>25-28</sup>

$$\frac{1}{L}E_g(L) \cong \varepsilon_\infty - \frac{\pi c v_s}{6L^2}, \quad (16)$$

where

$$v_s = \lim_{L \rightarrow \infty} \frac{L}{2\pi} \{E_{k_1}(L) - E_g(L)\}. \quad (17)$$

Here  $E_{k_1}(L)$  is the energy of the excited state with wave number  $k_1 = \frac{2\pi}{L}$  and magnetization  $M = 0$ . In general, we should obtain  $v_s$  as

$$v(L) = v_s + C_1/L^2 + C_2/L^4. \quad (18)$$

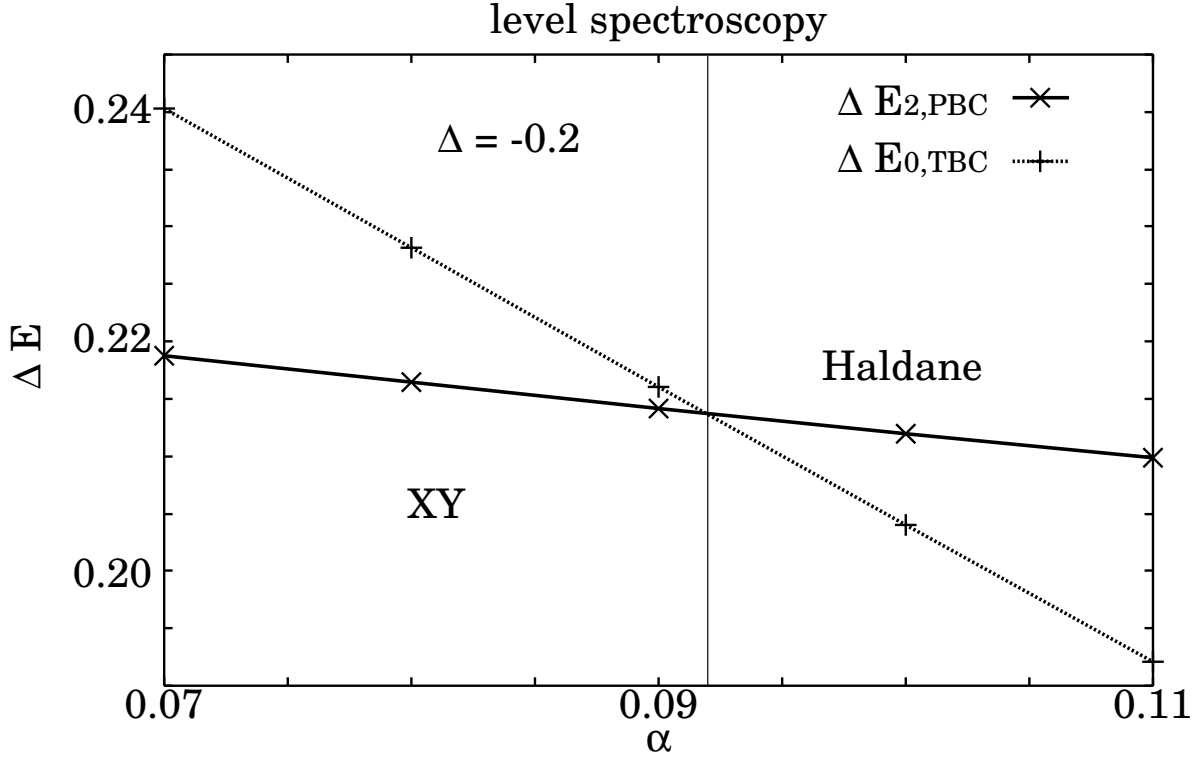


Fig. 2. This figure shows the energy level crossing between the  $x_{2,0}$  and the  $x_{0,0,odd}^{TBC}$ . When  $L = 16$  and  $\Delta = -0.2$ ,  $\alpha_c = 0.09193$ .

Although there remain logarithmic corrections in the central charge, which is obtained from eq. (16), they are small enough  $O(1/(\ln L)^3)$ .<sup>29</sup> Thus we can neglect them. Of course, the effective central charge  $\tilde{c}$  corresponds to the central charge  $c$  in the massless region. In the massive region, the correction term in eq. (16) is modified as  $1/L^2 \rightarrow \exp(-L/\xi)$ . We calculate the effective central charge  $\tilde{c}$ , which is shown in Fig. 4. We can see that the central charge changes rapidly from  $c = 1$  (massless) to  $\tilde{c} = 0$  (massive). This fact agrees with the previous results in refs.[30,31].

Then, we examine the ratio of the energy levels, in order to check the consistency. From eqs. (8) and (9),

$$\frac{\Delta E_2}{\Delta E_1} = 4, \quad (19)$$

where  $\Delta E_i = E(M = \pm i) - E_g(M = 0)$ ,  $i = 1, 2$ . This relation is independent of  $K$ . In the gapful (massive) phase, on the other hand, since the mass of the two magnons is twice that of one magnon when each magnons are independent, thus

$$\frac{\Delta E_2}{\Delta E_1} \rightarrow 2 \quad (L \rightarrow \infty). \quad (20)$$

The extrapolation is as follows.

$$\mathcal{O} = \mathcal{O}_\infty + C_1/L^2 + C_2/L^4, \quad (21)$$

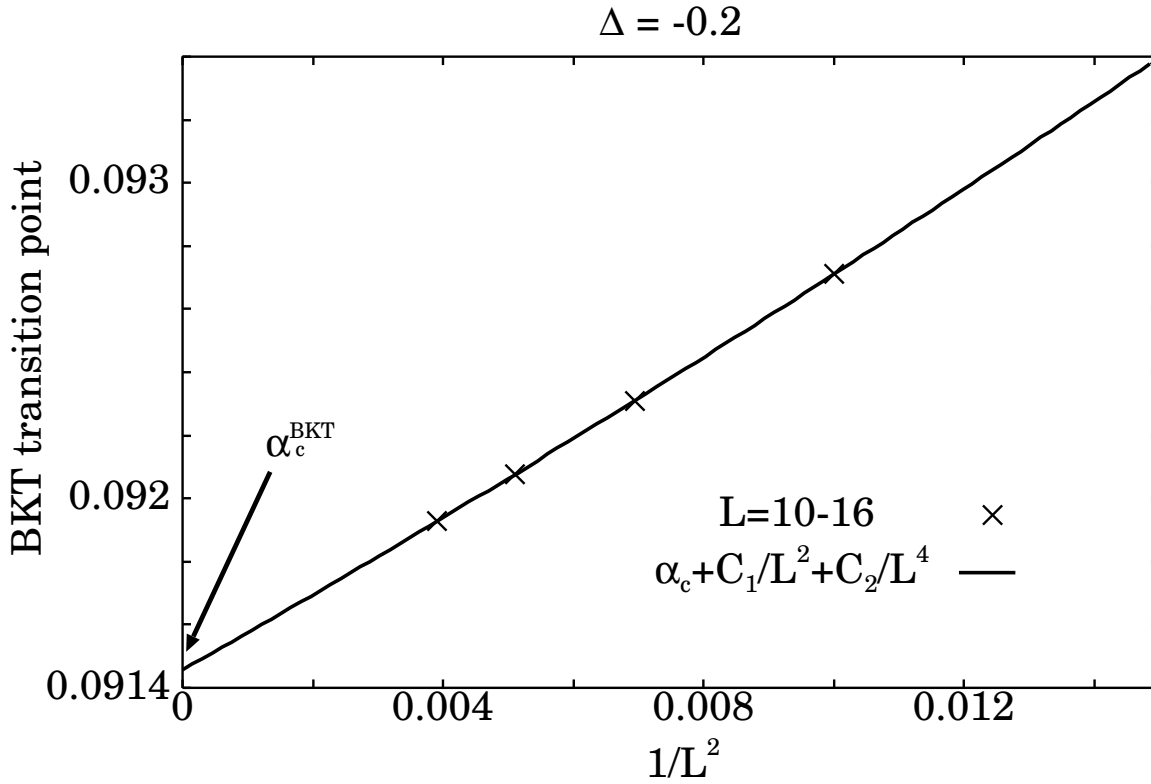


Fig. 3. The extrapolation procedure of  $\alpha_c^{\text{BKT}}$  for  $\Delta = -0.2$ . We suppose a fitting function as  $\alpha(L) = \alpha_c + C_1/L^2 + C_2/L^4$ .

where  $\mathcal{O}$  means  $\Delta E_2/\Delta E_1$ . We show this ratio in Fig. 5. We can also see the size dependency of the change of these states. It appears that the ratio is 4 in the massless phase and the ratio change from 4 to 2 is very slow because of the finite size effect.

### 3.2 instability of ferromagnetic phase

We determine the unstable boundary of the ferromagnetic phase as follows. If there is no intermediate phase, the transition from the  $M = \pm L$  (ferro) state to the  $M = 0$  state occurs via the energy level crossing. Thus, we can obtain the boundary of the ferromagnetic phase from the energy level crossing between the energy of the fully magnetized state (ferro),  $E = (1 + \alpha)\Delta L$ , and that of the  $M = 0$  state. We will compare the numerical result with the ferromagnetic spin wave theory (see APPENDIX A).

The phase diagram, determined by these two method, near the ferromagnetic phase is shown in Fig. 6. Below  $\alpha = 0.38$ , the ferromagnetic stable line from the diagonalization data is consistent with the line determined by the spin wave theory. The convergence of the diagonalization data is not so good above  $\alpha = 0.38$ .

We think that the incommensurability begins to influence the convergence of the ground state energy near the  $\alpha = 0.38$ . The behavior of the ferromagnetic phase boundary, represented by the energy level crossing from the diagonalization data, however, is analogous to that of

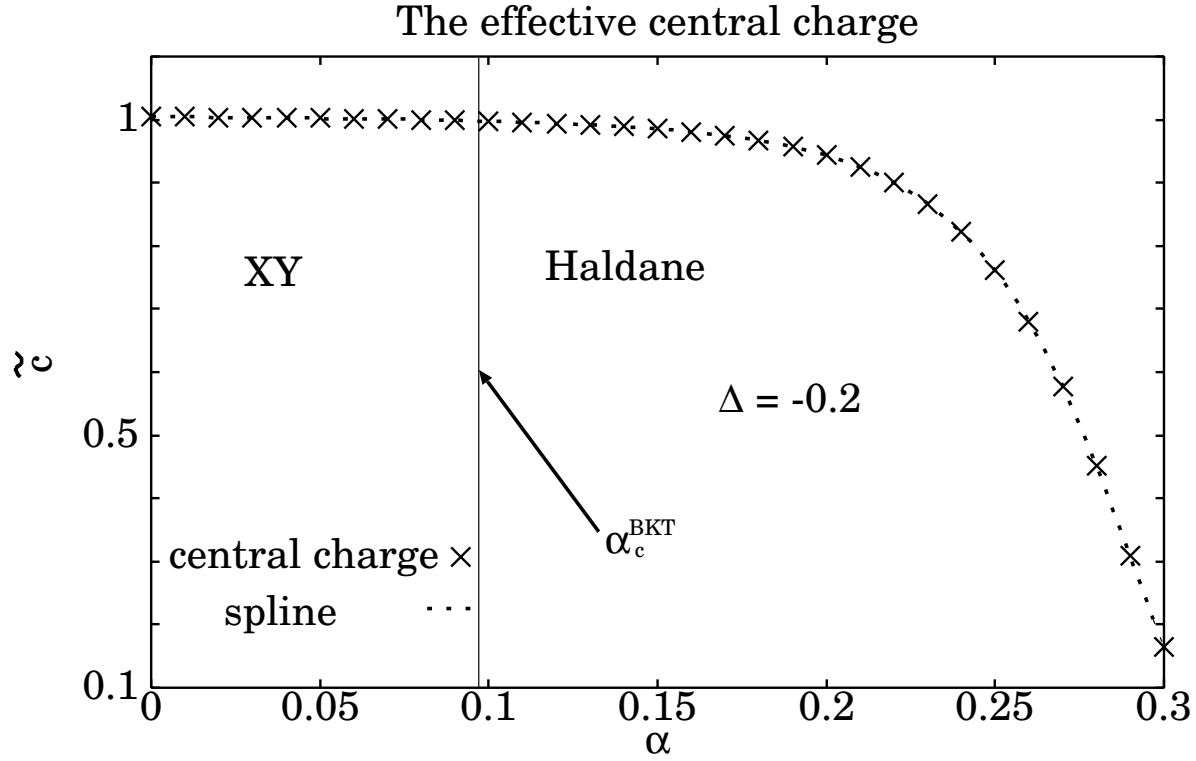


Fig. 4. The effective central charge  $c = 1$  in the massless region. This data is plotted for  $\Delta = -0.2$ . The BKT transition occurs at  $\alpha_c^{BKT}$ .

the spin wave theory. So that, in this work, we adopt the line of the spin wave theory as the ferromagnetic phase boundary in Fig. 1.

### 3.3 Haldane-Néel transition

The phase transition between the Haldane phase and the Néel phase belongs to the second order phase transition. In order to determine the transition line between the Haldane phase and the Néel phase, we apply the phenomenological renormalization group (PRG) method.<sup>20,21</sup> This method is explained as follows. In the Néel phase, the ground state is twofold degenerate in the thermodynamic limit. For finite  $L$ , however, this degeneracy is split into the small energy gap  $\Delta E(L, \alpha, \Delta)$ ,

which follows as  $\Delta E \sim \exp(-L/\xi)$ . On the other hand, the Haldane state has the energy gap, which remains finite in the thermodynamic limit. Thus the product  $L\Delta E(L)$  increases (decreases) with  $L$  for  $\Delta < \Delta_c^{HN}$  ( $\Delta > \Delta_c^{HN}$ ) where  $\Delta_c^{HN}$  means the critical value of  $\Delta$  of the Haldane-Néel transition. Therefore, we use the following equation to determine the the Haldane-Néel transition:

$$L\Delta E(L, \alpha, \Delta_c(L, L+2)) = (L+2)\Delta E(L+2, \alpha, \Delta_c(L, L+2)). \quad (22)$$

The finite-size transition point  $\Delta_c(L, L+2)$  is determined as shown in Fig. 7. Then, we

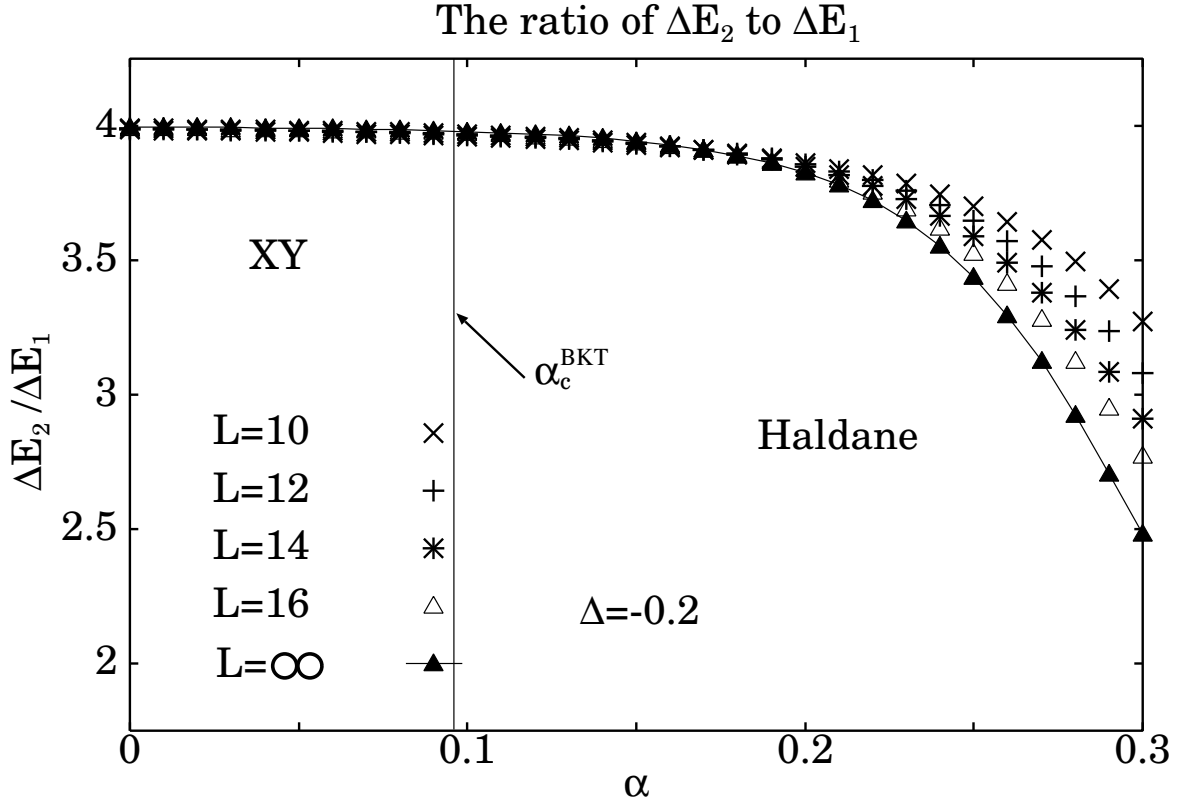


Fig. 5. We calculate  $\Delta E_2/\Delta E_1$ . In the XY phase,  $\Delta E_2/\Delta E_1 = 4$ , and  $\Delta E_2/\Delta E_1 = 2$  in the gapful phase. Because of the finite size effect,  $\Delta E_2/\Delta E_1$  varies slowly.

extrapolate the infinite-size critical point  $\Delta_c^{HN}$  as follows:

$$\Delta_c(L, L+2) = \Delta_c^{HN} + \frac{C_1}{(L+1)^2} + \frac{C_2}{(L+1)^4}. \quad (23)$$

When  $\alpha = -0.5$ , the infinite-size transition point  $\Delta_c^{HN}$  is determined as shown in Fig. 8. The same procedure can be carried out varying  $\Delta$  with fixed  $\alpha$ .

The obtained Haldane-Néel transition line is shown in Fig. 9. From the quantum Monte Carlo simulation at the  $\alpha = 0$ ,<sup>13</sup> this transition has been known to belong to the 2D-Ising type universality class. Therefore, we expect that the universality class of the whole Haldane-Néel transition line is of the 2D-Ising type.

#### 4. The analysis of the anisotropic non-linear $\sigma$ model

Now we examine the region for  $\alpha < 0$  near the  $\Delta = 1$ . In this region, we do not know whether the Haldane phase exists intermediately or the phase transition occurs directly between the XY phase and the Néel phase. From the numerical data, the BKT transition line and the 2D-Ising type transition line are very close near  $\Delta = 1$  for  $\alpha \ll 0$ . These two lines have some possibilities, being asymptotic, crossing or overlap, and so on. We can not distinguish numerically them because of the finite size effect.

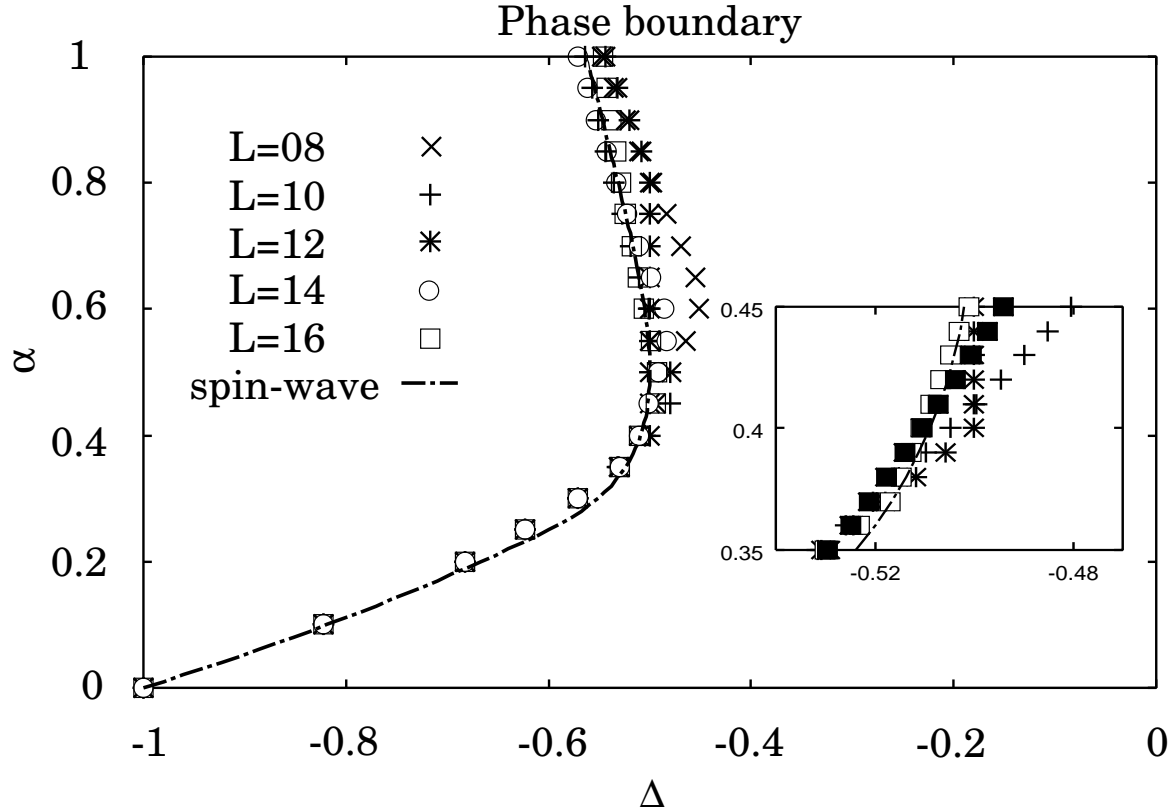


Fig. 6. This figure shows the phase boundary of the ferromagnetic phase, represented by the energy level crossing from the diagonalization data and the spin wave theory.

Therefore we argue this region analytically. We map the  $S = 1$  XXZ spin model onto the non-linear  $\sigma$  model with anisotropy in the large- $s$  limit<sup>32–35</sup> (see APPENDIX B). From the renormalization group equation (eq. (B-18)), the renormalization group flows are represented by  $\Delta$  and  $\alpha$  as

$$|\Delta - 1| \propto \frac{\sqrt{1 - 4\alpha}}{1 - \alpha} \exp(-2\pi\sqrt{1 - 4\alpha}), \quad \text{for } |\Delta - 1| \ll 1. \quad (\text{B-20})$$

We assume that these renormalization group flows are connected to the each renormalization group fixed points; the XY and the Ising fixed point. These fixed points will be asymmetric on the phase diagram. Therefore, we can draw the schematic phase diagram, compared with the numerical data, shown in Fig. 10. The numerical results are in good agreement with the analytical lines near  $\Delta = 1$  for  $\alpha \ll 0$ .

At the isotropic point,  $\Delta = 1$  and  $\alpha \rightarrow -\infty$ , the phase is massive, since the mass term (eq. (B-19)) exists. So, we conclude that there does not occur the phase transition between the XY phase and the Néel phase directly.

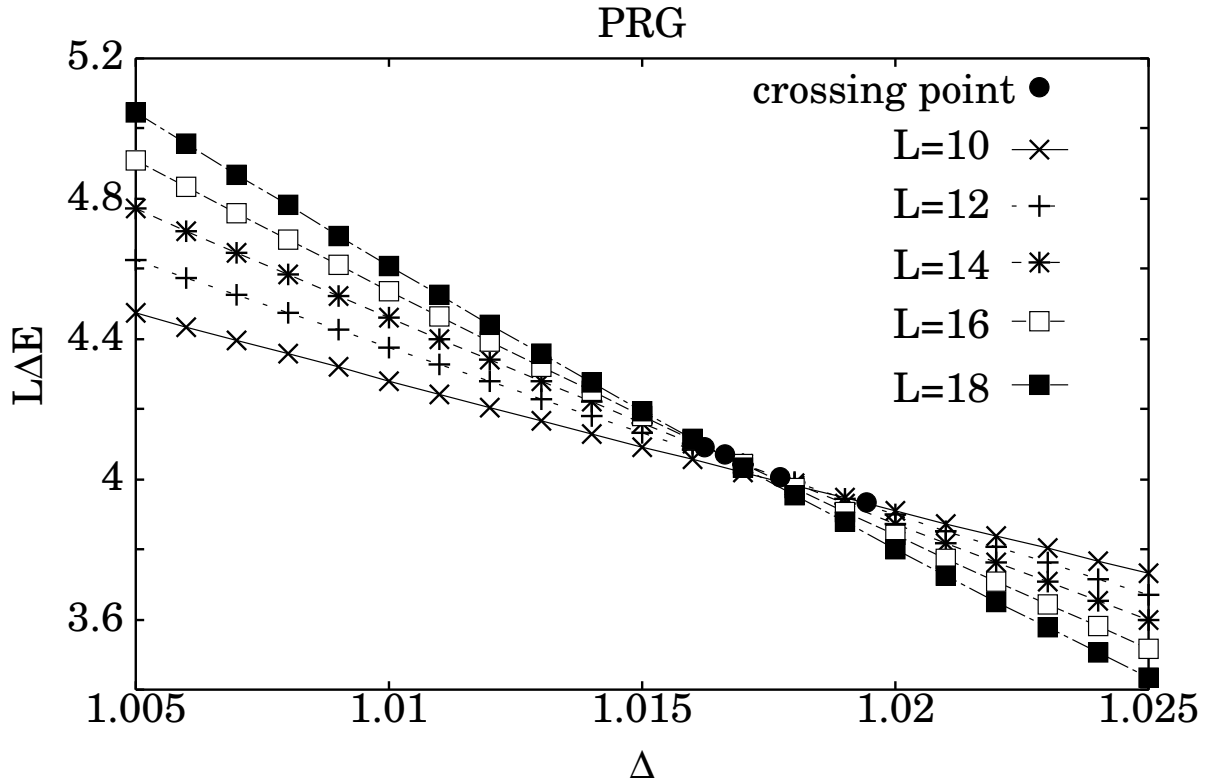


Fig. 7. The  $\Delta$  dependence of  $L\Delta E(L)$  with  $\alpha = -0.5$  for  $L = 10, 12, 14, 16$  and  $18$ . The intersections( $\bullet$ ) are the finite-size transition points.

## 5. SUMMARY AND DISCUSSION

The ground-state phase diagram of the  $S = 1$  XXZ chain with next-nearest-neighbor interaction is determined by analyzing the numerical diagonalization data using the level spectroscopy with the twisted boundary method, the phenomenological renormalization group, the finite-size scaling, the spin wave theory and the renormalization group. Particularly, it is resolved that the phase transition between the XY phase and the Néel phase does not occurs directly near  $\Delta = 1$  for  $\alpha \ll 0$ .

In this paper, we do not treat the region for  $\alpha \gtrsim 0.4$ , except for the vicinity of the ferromagnetic phase, because of the incommensurability. When  $\Delta = 1.0$ , the commensurate-incommensurate change occurs near  $\alpha = 0.38$ .<sup>36</sup> Since the incommensurability influence the numerical diagonalization, the analysis of the numerical diagonalization for finite-size  $L$  is failed in the region for  $\alpha \gtrsim 0.4$ . We can see the commensurate-incommensurate change.<sup>8,9,37,38</sup> However, this change is not a phase transition. We can not, so far, analyze the ground state in the incommensurate region by the exact diagonalization. In this region, the DMRG methods are known to be useful. In order to advance the analysis of the incommensurate region, we must find the effective method to treat this nasty problem.

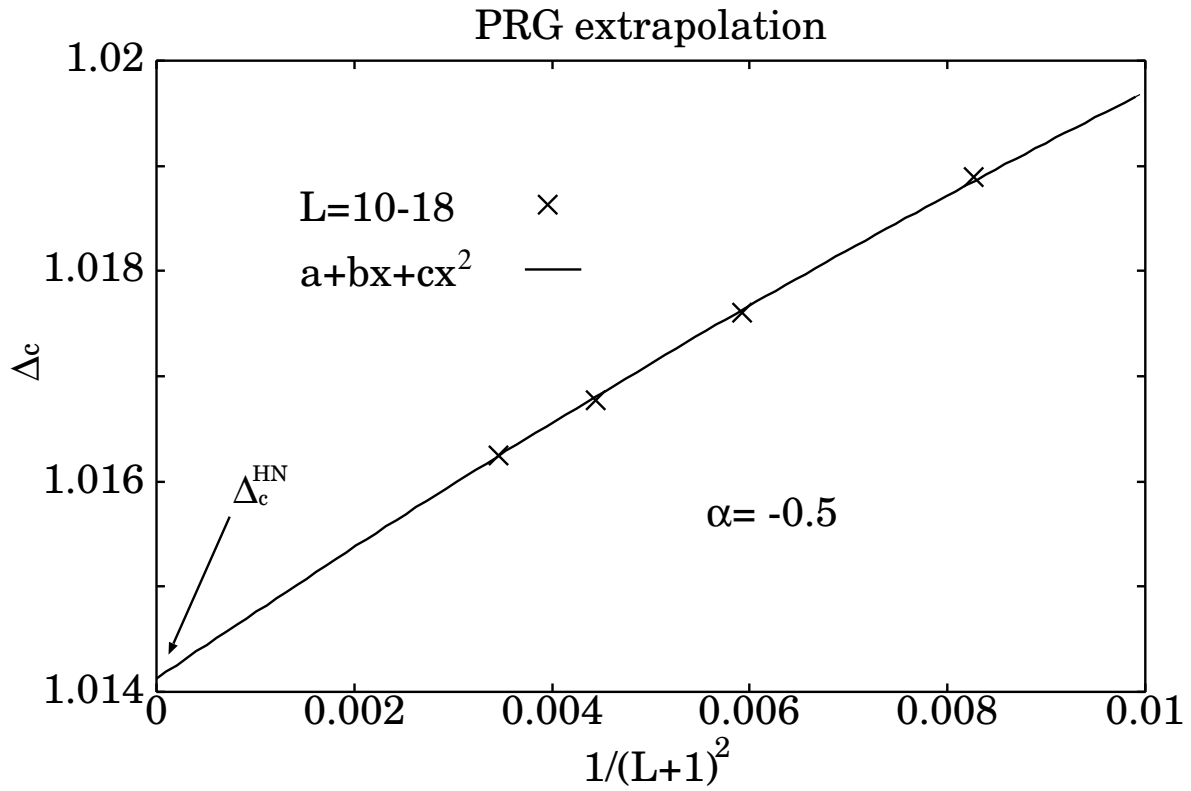


Fig. 8. We suppose a fitting function as  $\Delta_c(L, L+2) = \Delta_c^{HN} + C_1/(L+1)^2 + C_2/(L+1)^4$ .

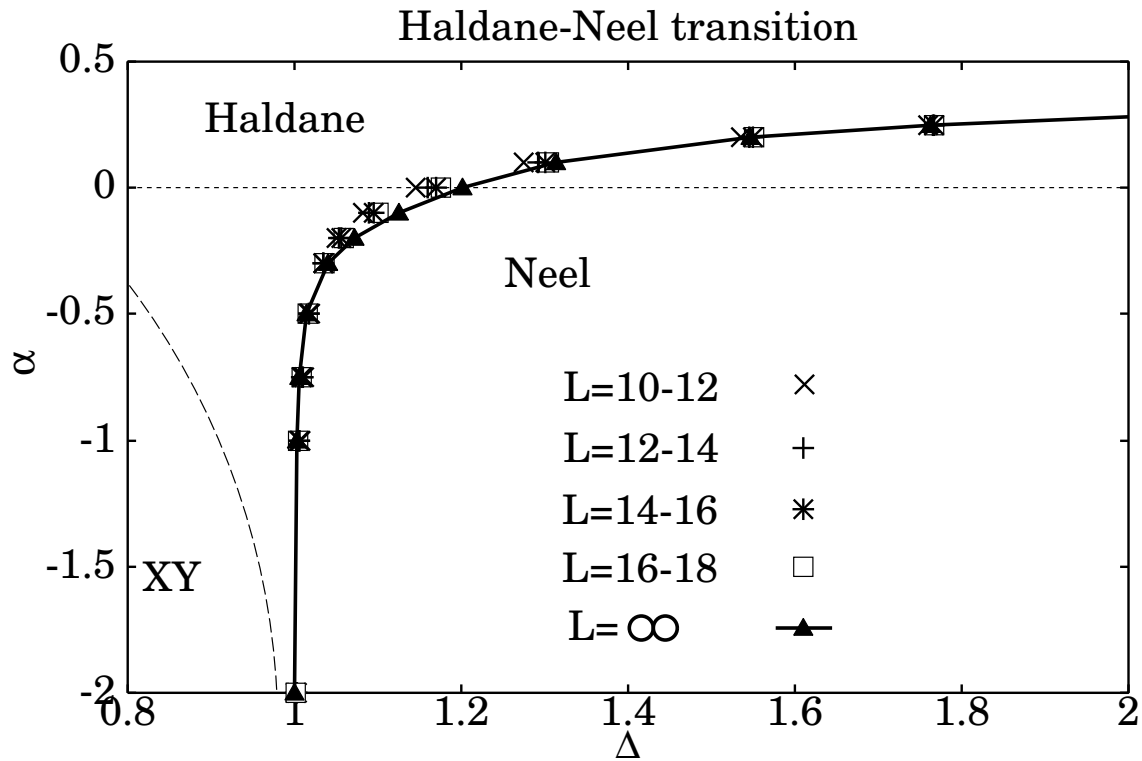


Fig. 9. The Phase diagram near the Haldane-Néel transition line.

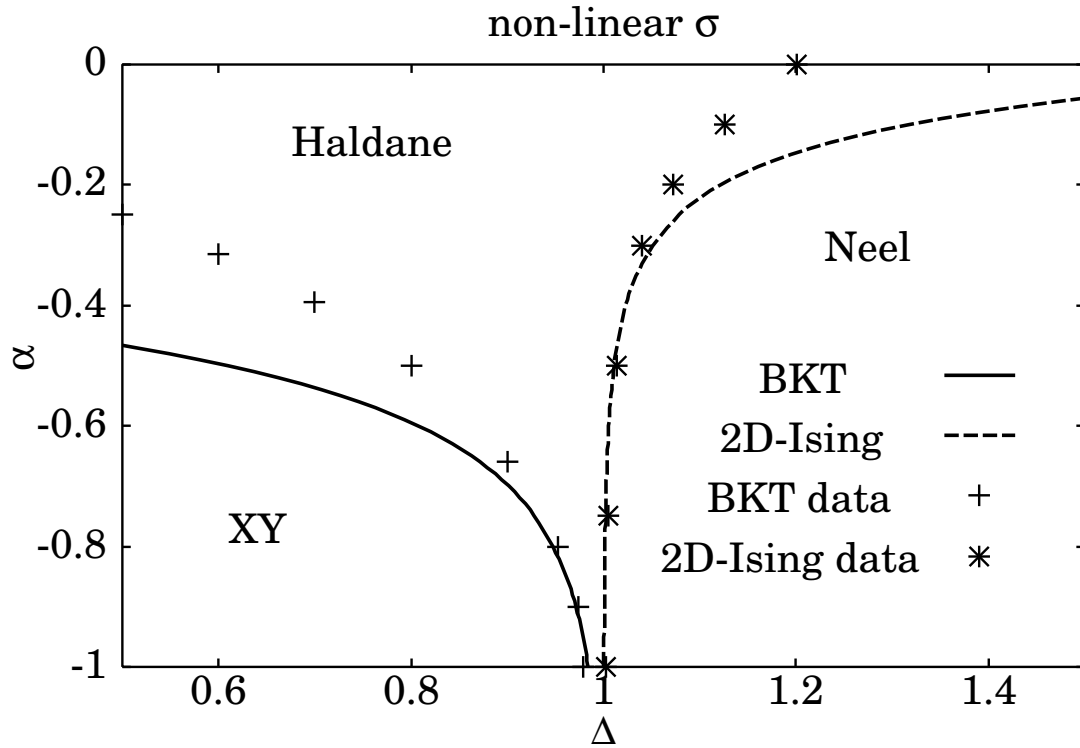


Fig. 10. From eq. (B·20), we can draw the schematic phase diagram near the  $\alpha = -1$  and  $\Delta = 1$  point. At the point, the phase is massive. We compare the schematic phase diagram with the numerical data in this figure. We use the extrapolated data ( $L = \infty$  in Fig. 9). The numerical results are in good agreement with the analytical lines near  $\Delta = 1$  and  $\alpha = -1$ .

### Acknowledgments

The numerical calculation in this work is based on the program packages TITPACK version 2, developed by Professor H. Nishimori, and KOBEPACK/S, coded by Professor M. Kaburagi. This work is partly supported by a Grant-in-Aid for Scientific Research on Priority Areas (B) ('Field-Induced New Quantum Phenomena in Magnetic Systems') from the Ministry of Education, Culture, Sports, Science and Technology of Japan. We further thank the Supercomputer Center, Institute for Solid State Physics, University of Tokyo, the Information Synergy Center, Tohoku University, and the Computer Room, Yukawa Institute for Theoretical Physics, Kyoto University for computational facilities.

### Appendix A: The analysis of spin wave instability

In this Appendix, we consider the instability analysis of the ferromagnetic phase of the one dimensional spin- $s$  XXZ chain with the next-nearest-neighbor interaction. We consider the Hamiltonian as follows,

$$\mathcal{H} = \sum_{i=1}^L (S_i^x S_{i+1}^x + S_i^y S_{i+1}^y + \Delta S_i^z S_{i+1}^z)$$

$$+\alpha \sum_{i=1}^L (S_i^x S_{i+2}^x + S_i^y S_{i+2}^y + \Delta S_i^z S_{i+2}^z), \quad (\text{A}\cdot 1)$$

where  $\alpha$  is the next-nearest-neighbor interaction,  $S_i^x, S_i^y$  and  $S_i^z$  are the spin- $s$  operators at the  $i$ th site, and  $L$  is the system size. We assume the periodic boundary condition ( $S_{i+L}^\gamma = S_i^\gamma, \gamma = \{x, y, z\}$ ).

We denote the fully ferromagnetic state by  $|0\rangle$ . In this state, all spins have the eigen value  $s$  for  $S^z$ . Then,

$$S_i^+ |0\rangle = 0 \quad (\text{for } \forall i\text{-th site}). \quad (\text{A}\cdot 2)$$

Since the state  $|0\rangle$  is the eigenvector of the Hamiltonian, we obtain the eigen value of the Hamiltonian;

$$\mathcal{H}|0\rangle = E_0|0\rangle, \quad (\text{A}\cdot 3)$$

$$E_0 = \Delta s^2 L + \alpha \Delta s^2 L. \quad (\text{A}\cdot 4)$$

The fully ferromagnetic state  $|0\rangle$  is the ground state for the fully ferromagnetic phase.

In order to see the lowest excitation, we consider the following operator which is the linear combination of the spin lowering operator,

$$\sum_m S_m^- \exp(-ikm), \quad (\text{A}\cdot 5)$$

where  $k$  is the wave number. When this operator act on  $|0\rangle$ , we obtain the following eigen value,

$$\mathcal{H} \sum_m S_m^- \exp(-ikm) |0\rangle = \{E_0 + \omega(k)\} \sum_m S_m^- \exp(-ikm) |0\rangle. \quad (\text{A}\cdot 6)$$

where  $\omega(k)$  represents the dispersion relation,

$$\omega(k) = 2s\{(\cos k - \Delta) + \alpha(\cos 2k - \Delta)\} \quad (\text{A}\cdot 7)$$

$$= 2s \left\{ 2\alpha \left( \cos k + \frac{1}{4\alpha} \right)^2 - \frac{1}{8\alpha} - \alpha - \Delta - \alpha\Delta \right\}. \quad (\text{A}\cdot 8)$$

If  $\omega(k)$  is negative, the fully ferromagnetic state is unstable because of the spin wave excitation. Since the prefactor  $2s$  is positive, we omit  $2s$  in the following analysis.

In order to examine the incommensurate region, we consider for  $\alpha > 0$ . If  $\omega(\cos k = -\frac{1}{4\alpha}) \geq 0$  for  $\alpha > 1/4$ , the ferromagnetic phase is stable. When  $\cos k = \frac{-1}{4\alpha}$ ,

$$\omega \left( \pm \arccos \frac{-1}{4\alpha} \right) = -\frac{1}{8\alpha} - \alpha - \Delta - \alpha\Delta. \quad (\text{A}\cdot 9)$$

When the right hand is zero,

$$\Delta = -\frac{1 + 8\alpha^2}{8\alpha(1 + \alpha)}. \quad (\text{A}\cdot 10)$$

Then the fully ferromagnetic phase becomes unstable for  $k = \pm \arccos \frac{-1}{4\alpha}$  mode of the spin wave excitation.

Next, we consider for  $\alpha < \frac{1}{4}$ . If  $\omega(k = \pm\pi) \geq 0$ , the ferromagnetic phase is stable. When  $k = \pm\pi$ ,

$$\omega(\pm\pi) = -1 - \Delta + \alpha - \alpha\Delta. \quad (\text{A}\cdot 11)$$

When the right hand is zero,

$$\Delta = \frac{\alpha - 1}{\alpha + 1}. \quad (\text{A}\cdot 12)$$

Then the fully ferromagnetic phase becomes unstable for  $k = \pm\pi$  mode of the spin wave excitation.

### Appendix B: non-linear sigma model

The one dimensional quantum spin- $s$  XXZ chain can be mapped onto the non-linear  $\sigma$  model with the anisotropy in the large- $s$  limit.<sup>33-35</sup>

At first, we consider the antiferromagnetic Heisenberg Hamiltonian with the next-nearest-neighbor interaction. The Hamiltonian is as follows,

$$\mathcal{H} = \sum_i \mathbf{S}_i \cdot \mathbf{S}_{i+1} + \alpha \sum_i \mathbf{S}_i \cdot \mathbf{S}_{i+2} \quad (\text{B}\cdot 1)$$

with  $\alpha < 0$ . Now we want to keep low energy modes as follows,

$$\mathbf{S}_i \simeq (-1)^i s\boldsymbol{\varphi}_i + a\mathbf{l}_i, \quad (\text{B}\cdot 2)$$

where  $\boldsymbol{\varphi}$  corresponds to the Fourier mode with the wave number  $k \simeq \pi$ , and  $\mathbf{l}$  corresponds to the Fourier mode with the wave number  $k \simeq 0$ . Here we define the following operators,

$$\boldsymbol{\varphi}\left(2i + \frac{1}{2}\right) = \frac{(\mathbf{S}_{2i+1} - \mathbf{S}_{2i})}{2s}, \quad (\text{B}\cdot 3)$$

$$\mathbf{l}\left(2i + \frac{1}{2}\right) = \frac{(\mathbf{S}_{2i+1} + \mathbf{S}_{2i})}{2a}. \quad (\text{B}\cdot 4)$$

where  $a$  is the lattice spacing,  $\boldsymbol{\varphi}$  and  $\mathbf{l}$  are slowly varying on the scale of the lattice spacing.

In the continuous limits, these operators are obeying the following commutators,

$$[l^\alpha(x), l^\beta(y)] = i\varepsilon^{\alpha\beta\gamma} l^\gamma(x) \delta(x - y), \quad (\text{B}\cdot 5)$$

$$[l^\alpha(x), \varphi^\beta(y)] = i\varepsilon^{\alpha\beta\gamma} \varphi^\gamma(x) \delta(x - y), \quad (\text{B}\cdot 6)$$

$$[\varphi^\alpha(x), \varphi^\beta(y)] = i\varepsilon^{\alpha\beta\gamma} l^\gamma(x) \delta(x - y) 2a \frac{1}{4s^2} \rightarrow 0, \quad (\text{B}\cdot 7)$$

where  $\{\alpha, \beta, \gamma\} = \{x, y, z\}$  and  $\varepsilon^{\alpha\beta\gamma}$  is the three-dimensional Levi-Civita symbol. Repeated indices are normally summed. These operators are obeying the constraints,

$$\boldsymbol{\varphi} \cdot \mathbf{l} = 0, \quad (\text{B}\cdot 8)$$

$$|\boldsymbol{\varphi}|^2 = 1. \quad (\text{B}\cdot 9)$$

Now the Hamiltonian density can be mapped onto the  $O(3)$  non-linear  $\sigma$  model,

$$\mathcal{H} = \frac{v}{2} \left\{ g \left( 1 - \frac{\theta}{4\pi} \frac{\partial \varphi}{\partial x} \right)^2 + \frac{1}{g} \left( \frac{\partial \varphi}{\partial x} \right)^2 \right\}, \quad (\text{B}\cdot 10)$$

where the velocity  $v = 2sa$ , the topological angle  $\theta = 2\pi s$  and the coupling constant  $g = \frac{2}{s\sqrt{1-4\alpha}}$ .

At second, we consider the Hamiltonian with the anisotropy as follows,

$$\mathcal{H} = \sum_i \mathbf{S}_i \cdot \mathbf{S}_{i+1} + \alpha \sum_i \mathbf{S}_i \cdot \mathbf{S}_{i+2} + \sum_i \{ (\Delta - 1) S_i^z S_{i+1}^z + \alpha (\Delta - 1) S_i^z S_{i+2}^z \}. \quad (\text{B}\cdot 11)$$

In this case, we obtain the following effective Hamiltonian density,

$$\mathcal{H} = \frac{v}{2} \left\{ g \left( 1 - \frac{\theta}{4\pi} \frac{\partial \varphi}{\partial x} \right)^2 + \frac{1}{g} \left( \frac{\partial \varphi}{\partial x} \right)^2 \right\} + \frac{vm^2}{2g} \varphi_z^2, \quad (\text{B}\cdot 12)$$

where

$$m^2 = \frac{2(\Delta - 1)(-1 + \alpha)}{a^2(1 - 4\alpha)^{1/2}}. \quad (\text{B}\cdot 13)$$

When we map (B·11) onto (B·12), we chose the leading term in the anisotropic terms as

$$S_i^z S_{i+1}^z \sim -s^2 \varphi_z^2 \quad (\text{B}\cdot 14)$$

and

$$S_i^z S_{i+2}^z \sim s^2 \varphi_z^2. \quad (\text{B}\cdot 15)$$

In this case, we can apply to the renormalization group equation obtained by Nelson and Pelcovits.<sup>32</sup> Since we take  $d = 2, N = 3$  case, we obtain

$$\frac{dg}{d \ln b} = \frac{1}{2\pi} \left( \frac{g^2}{1 + m^2} \right), \quad (\text{B}\cdot 16)$$

$$\frac{dm^2}{d \ln b} = 2m^2 - \frac{1}{\pi} \frac{gm^2}{1 + m^2}. \quad (\text{B}\cdot 17)$$

Then we can obtain the following differential equation,

$$\frac{dm^2}{dg} = \frac{4\pi}{g^2} m^2 (1 + m^2) - \frac{2m^2}{g}. \quad (\text{B}\cdot 18)$$

From this equation we obtain the following solution

$$m^2(g) \propto \exp \left( -\frac{4\pi}{g} \right). \quad (\text{B}\cdot 19)$$

From eqs. (B·13) and (B·19), therefore, we obtain the relation between  $\Delta$  and  $\alpha$  as

$$|\Delta - 1| \propto \frac{a^2 \sqrt{1 - 4\alpha}}{2(1 - \alpha)} \exp(-2\pi \sqrt{1 - 4\alpha}). \quad (\text{B}\cdot 20)$$

Note that eq. (B·20) can be extended to the  $\alpha \rightarrow -\infty$  limit.

**References**

- 1) F. D. M. Haldane: Phys. Lett. **93A** (1983) 464.
- 2) F. D. M. Haldane: Phys. Rev. Lett. **50** (1983) 1153.
- 3) H. Kikuchi, M. Chiba and T. Kubo: Can. J. Phys. **79** (2001) 1551.
- 4) T. Masuda, T. Sakaguchi and K. Uchinokura: J. Phys. Soc. Jpn. **71** (2002) 2637.
- 5) T. Tonegawa, S. Suzuki and M. Kaburagi: J. Magn. Magn. Mater. **140-144** (1995) 1613.
- 6) M. Kaburagi, H. Kawamura and T. Hikihara: J. Phys. Soc. Jpn. **68** (1999) 3185.
- 7) T. Hikihara, M. Kaburagi, H. Kawamura and T. Tonegawa: J. Phys. Soc. Jpn. **69** (2000) 259.
- 8) A. Kolezhuk, R. Roth and U. Schollwöck: Phys. Rev. Lett. **25** (1996) 5142.
- 9) A. Kolezhuk, R. Roth and U. Schollwöck: Phys. Rev. B **55** (1997) 8928.
- 10) A. Kitazawa, K. Nomura and K. Okamoto: Phys. Rev. Lett. **76** (1996) 4038.
- 11) A. Kitazawa and K. Nomura: J. Phys. Soc. Jpn. **66** (1997) 3944.
- 12) W. Chen, K. Hida and B. C. Sanctuary: Phys. Rev. B **67** (2003) 104401.
- 13) K. Nomura: Phys. Rev. B **40** (1989) 9142.
- 14) P. Lecheminant, T. Jolicoeur and P. Azaria: Phys. Rev. B **63** (2001) 174426.
- 15) A. Kitazawa, K. Hijii and K. Nomura: J. Phys. A **36** (2003) L351.
- 16) K. Nomura and K. Okamoto: J. Phys. A **27** (1994) 5773.
- 17) K. Nomura: J. Phys. A **28** (1995) 5451.
- 18) A. Kitazawa: J. Phys. A **30** (1997) L285.
- 19) K. Nomura and A. Kitazawa: J. Phys. A **31** (1998) 7341.
- 20) M. N. Barber: Phase transition and Critical Phenomena, ed. C. Domb and J. L. Lebowitz (ACADEMIC PRESS, 1983) Vol. 8, p. 145.
- 21) H. H. Roomany and H. W. Wyld: Phys. Rev. D **21** (1980) 3341.
- 22) H. J. Schulz: Phys. Rev. B **34** (1986) 6372.
- 23) J. M. Kosterlitz: J. Phys. C **7** (1974) 1046.
- 24) L. P. Kadanoff and A. C. Brown: Ann. Phys. **121** (1979) 318.
- 25) J. L. Cardy: J. Phys. A **17** (1984) L385.
- 26) J. L. Cardy: Nucl. Phys. B **270**[FS16] (1986) 186.
- 27) H. W. Blöte, J. L. Cardy and M. P. Nightingale: Phys. Rev. Lett. **56** (1986) 742.
- 28) I. Affleck: Phys. Rev. Lett. **56** (1986) 746.
- 29) J. L. Cardy: J. Phys. A **19** (1986) L1093.
- 30) H. Inoue and K. Nomura: Phys. Lett. A **262** (1999) 96.
- 31) H. Inoue: Phys. Lett. A **270** (2000) 359.
- 32) D. R. Nelson and R. A. Pelcovits: Phys. Rev. B **16** (1977) 2191.
- 33) I. Affleck: Phys. Rev. Lett. **56** (1986) 408.
- 34) I. Affleck: J. Phys. Cond. Matt. **1** (1989) 3047.
- 35) I. Affleck: Fields, Strings and Critical Phenomena Les Houches XLIX 1988, ed. E. Brezin and J. Zinn-Justin (Amsterdam: North-Holland, 1990) p. 563.
- 36) T. Tonegawa, M. Kaburagi, N. Ichikawa and I. Harada: J. Phys. Soc. Jpn. **61** (1992) 2890.
- 37) T. Tonegawa and I. Harada: J. Phys. Soc. Jpn. **56** (1987) 2153.
- 38) K. Nomura: J. Phys. Soc. Jpn. **72** (2003) 476.